

Research Article

Vibration Control of Manipulators with Flexible Nonprismatic Links Using Piezoelectric Actuators and Sensors

**Valdecir Bottega,¹ Alexandre Molter,² Jun S. O. Fonseca,²
and Rejane Pergher¹**

¹ *Department of Mathematics and Statistics, University of Caxias do Sul (UCS),
R. Francisco Getúlio Vargas, 1130, 95570-560 Caxias do Sul, RS, Brazil*

² *Department of Mechanical Engineering, Federal University of Rio Grande do Sul (UFRGS), Sarmiento
Leite, 425, 90050-170 Porto Alegre, RS, Brazil*

Correspondence should be addressed to Valdecir Bottega, vbottega@ucs.br

Received 17 February 2009; Accepted 29 April 2009

Recommended by Mohammad Younis

This work presents a tracking control model for a flexible nonprismatic link robotic manipulator using simultaneously motor torques and piezoelectric actuators. The dynamic model of the flexible manipulator is obtained in a closed form through the Lagrange equations. The control uses the motor torques for the joints tracking control and also to reduce the low-frequency vibration induced in the manipulator links. The stability of this control is guaranteed by the Lyapunov stability theory. Piezoelectric actuators and sensors are added for controlling vibrations with frequencies beyond the reach of motor torque control. The natural frequencies are calculated by the finite element method, and the approximated eigenfunctions are interpolated by polynomials. Three eigenfunctions are used for the dynamics of the arm, while only two are used for the control. Numerical experiments on Matlab/Simulink are used to verify the efficiency of the control model.

Copyright © 2009 Valdecir Bottega et al. This is an open access article distributed under the Creative Commons Attribution License, which permits unrestricted use, distribution, and reproduction in any medium, provided the original work is properly cited.

1. Introduction

The need of lightweight robots has attracted the attention to robotic manipulators with flexible links. These robots are essential in mobile applications, such as surface vehicles, aircrafts, and spacecrafts. The design of these manipulators requires a control system which takes into account the interaction of the joint angles and the elastic modes. Modelling this control has the additional complication of the essential uncertainty that characterizes robotic manipulators, such as variable payload and joint frictional torques [1].

Designing a control for a flexible robot design requires two steps: a robust tracking control, acting on the joint angles, and a stabilizer for the motion-induced vibration

suppression. Robotic systems can be approximated as linear with respect to some parameters, as mass, inertia, and damping factors, but this assumption is too inaccurate for the state. Therefore, a position control law must be defined with an appropriate tracking error asymptotic stability, verified with Lyapunov functions [2].

A linearized model-based stabilizer is designed to damp the elastic oscillation [3]. However, the high-frequency modes cannot be eliminated by the motor action alone, because the torque control system low speed is ill suited for high-frequency vibrations. Thus, the control of those vibrations must use higher frequency actuators like piezoelectrics.

Piezoelectricity is defined as a relation between an applied electric field and strain or an applied strain and electric field in certain crystals, ceramics, and films. In general, flexible robot manipulators feature surface bonded or embedded piezoelectric actuators and or sensor. The piezoceramic actuator generates a large actuating force and has a fast response time. Moreover it is smaller than other actuating systems as electrical motor or hydraulics for the same force [4].

Robots' flexible links are built in complex geometries, which cannot be modeled by simple beam bending equations. In this work we propose a methodology for accounting the complex geometry within the realm of the Euler-Bernoulli beam theory.

The finite element method is used for the solution of the vibration eigenproblem since the analytical approach is cumbersome for complex nonprismatic beams. However, we wish to retain the simplicity of the analytic derivation of the control; the eigenvectors are interpolated from the nodal values with polynomials [5]. The effectiveness of this interpolation is checked by the Rayleigh quotient [6].

A piezoelectric actuator is applied to single-link flexible manipulators in [7, 8] and to two-link flexible manipulators in [9]. In these works, the control torque of the motor is determined based only on the rigid link dynamics, and all the oscillations are suppressed by applying a feedback control voltage to the piezoelectric actuator.

In this work, we propose a tracking control model for a robot arm with flexible links. Motor torques control based on the elastic link dynamics is used for the joint motion and reduces the low-frequency vibrations. The actuation frequencies ranges of the motor and piezoelectric inserts are chosen to be nonoverlapping, so that their controls are uncoupled.

The lower fundamental modes are responsible for the most of the tip displacement of the robot arm; therefore only the first three eigenfunctions are considered in the work. The theory formulated in this work can be use for more than one flexible link, but for simplification, the simulated model has one rigid and one flexible link. A Matlab/Simulink code was created to assess the control model efficiency.

2. Dynamic Model

The motion of the robot endpoint is a composition of the successive relative link motions. This movement is described using homogeneous matrix transformations. These transformations represent translations and rotations due to the joints angle change and the flexible link elastic deflections [10]. Flexible Links are modeled as Euler-Bernoulli beams, with vibration deflection $d_{yi}(x_i, t)$ satisfying the partial differential equation

$$(EI)_i \frac{\partial^4 d_{yi}(x_i, t)}{\partial x^4} + \rho_i a_i \frac{\partial^2 d_{yi}(x_i, t)}{\partial t^2} = p_i(x), \quad (2.1)$$

where ρ_i is the density, a_i is the cross-section, $p_i(x)$ are the external forces actuating on the beam, and $(EI)_i$ is the flexural rigidity constant of the i th link [11]. For small displacements, the natural frequencies and modes can be considered independent of the external forces.

Exploring the time and space separability on (2.1) by the modal analysis technique, the link deflection can be expressed as

$$d_{yi}(x_i, t) = \sum_{i=1}^{m_i} \varphi_{ij}(x_i) \delta_{ij}(t), \quad (2.2)$$

where each term in the general solution of (2.1) is the product of a time harmonic function of the term $\delta_{ij}(t) = e^{j\omega_{ij}t}$, and a space eigenfunction which for uniform cross section is written as

$$\begin{aligned} \varphi_{ij}(x_i) = & C_{1ij} \sin\left(\frac{\rho_i \omega_{ij}^2}{(EI)_i} x_i\right) + C_{2ij} \cos\left(\frac{\rho_i \omega_{ij}^2}{(EI)_i} x_i\right) + C_{3ij} \sinh\left(\frac{\rho_i \omega_{ij}^2}{(EI)_i} x_i\right) \\ & + C_{4ij} \cosh\left(\frac{\rho_i \omega_{ij}^2}{(EI)_i} x_i\right), \end{aligned} \quad (2.3)$$

where ω_{ij} is the j th natural angular frequency of the eigenvalue problem for link i , and m_i is the number of eigenfunctions considered in the truncated analysis. The determination of the constant coefficients C_{kij} uses clamped conditions at the link base and mass boundary conditions representing the balance of bending moment and shearing force at the link endpoint [12].

This solution is possible when the link geometry is prismatic or slightly nonprismatic. For irregular link shapes it is very difficult to obtain a closed form analytic solution; so we propose a more general approach in the next section.

3. Approximating Solutions for Eigenfunctions

The manipulators links are modeled as beams, since their lengths are usually much larger than the cross-sectional height and depth. Thereby, considering that the control can prevent large displacements, it is possible to apply the Euler-Bernoulli theory for small displacements, where (2.1) of motion for a single link is rewritten as

$$\frac{d^2}{dx^2} \left(EI \frac{d^2 \varphi_j}{dx^2} \right) = -\rho a \omega_j^2 \varphi_j, \quad (3.1)$$

Approximating φ_j by the finite element method requires firstly to write the weak form of the equation

$$\int_0^l \frac{d^2}{dx^2} \left(EI \frac{d^2 \varphi_j}{dx^2} \right) v \, dx + \int_0^l \rho a \omega_j^2 v \varphi_j = 0, \quad \forall v, \quad (3.2)$$

where v is an arbitrary variation of φ_j with $v(0) = 0$.

We assume admissible solution of the form

$$\begin{aligned}\varphi_j &= \sum_{I=1}^N Q_I \psi_I, \\ v &= \sum_{J=1}^N V_J \psi_J.\end{aligned}\tag{3.3}$$

where Q_I, V_J are scalar coefficients, and N are the number of basis functions $\{\psi_1, \psi_2, \dots, \psi_N\}$. The link is divided in several subdomains; the finite elements and these base functions are assumed to have compact support on a single element.

Recalling that EI is assumed constant on each finite element [5], using integration by parts, and substituting (3.3) in the results, we derive the expressions of the stiffness, mass and damping matrices, respectively,

$$\begin{aligned}K_{IJ} &= \int_0^l EI \frac{d^2\psi_I}{dx^2} \frac{d^2\psi_J}{dx^2} dx, \\ M_{IJ} &= \int_0^l \rho a \psi_I \psi_J dx, \\ \mathbf{C} &= \alpha \mathbf{M} + \beta \mathbf{K},\end{aligned}\tag{3.4}$$

where ψ are the elementwise interpolation functions, and α, β are the Rayleigh damping constants. Usually four cubic Hermite polynomials are used as interpolation functions in each two-node finite element; so the unknowns of the approximated problem are nodal displacements and its derivatives. The mass matrix can be further approximated by its lumped form. Then the natural modes and frequencies can be computed by the following matrix eigenvalue problem:

$$(\mathbf{K} - \omega_j^2 \mathbf{M}) \boldsymbol{\varphi}_j = 0,\tag{3.5}$$

where ω_j^2 are the characteristic values from (3.5). The eigenvectors represent the vibration modes in nodal coordinates.

Considering that the control algorithm requires twice differentiable eigenfunctions, it is necessary to create a continuous interpolation from the discrete values. The natural choice would be using the same elementwise Hermite polynomials used by the finite element approximation, but the eigenfunctions $\boldsymbol{\varphi}$ present large oscillations, due to excessive sensitivity to the numerical imprecision, specially of the derivatives. Figure 1 shows these oscillations for the first and second mass-normalized eigenfunction interpolation.

It is possible to smooth these disturbances by choosing another set of interpolation functions. In this case, we chose to forgo the elementwise Hermite approximation for a global interpolation ignoring the derivatives of the inner nodes. Three alternatives are considered: interpolating all nodes with a single Hermite approximation, a mixed Hermite-Lagrange set of polynomials which satisfies the displacements and derivatives at the outermost nodes, but only the displacements at the inner nodes, and finally a least-squares polynomial regression.

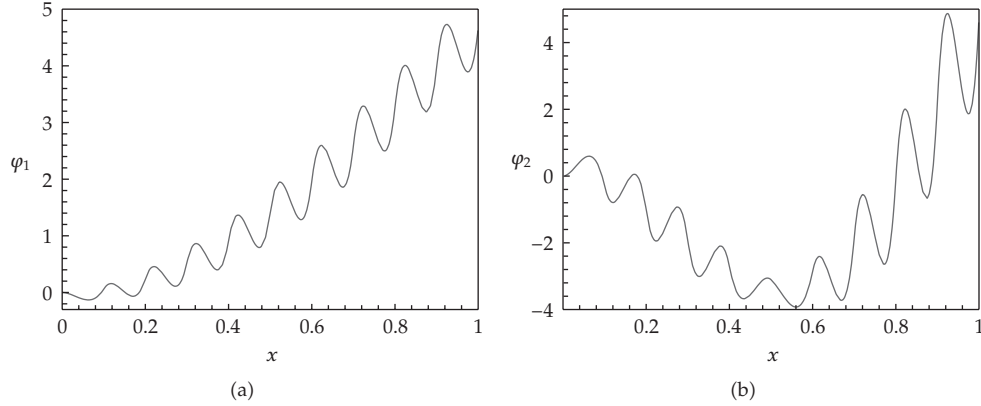


Figure 1: Eigenfunctions which represent the vibration modes of a link fixed on $x = 0$. (a) is the first mode and (b) the second mode. Eigenfunctions generate through the interpolation with Hermite polynomial in each element.

For computing the coefficients by least-squares it is necessary to consider the pseudoinverse operator \mathbf{A}^+ [13]. This operator has the following properties: if $\mathbf{A}^T \mathbf{A}$ is invertible, then $\mathbf{A}^+ = (\mathbf{A}^T \mathbf{A})^{-1} \mathbf{A}^T$; if $\mathbf{A} \mathbf{A}^T$ is invertible, then $\mathbf{A}^+ = \mathbf{A}^T (\mathbf{A} \mathbf{A}^T)^{-1}$. The coefficients from the polynomials are calculated from the results of the linear system $\mathbf{A} \mathbf{x} = \mathbf{y}$, hence $\mathbf{x} = \mathbf{A}^+ \mathbf{y}$.

The matrix \mathbf{A} comes from the finite element mesh and \mathbf{y} from the eigenvectors values:

$$\mathbf{A} = \begin{bmatrix} x_1^n & \cdots & x_1^1 & 1 \\ x_2^n & \cdots & x_2^1 & 1 \\ \vdots & \cdots & \vdots & \vdots \\ x_p^n & \cdots & x_p^1 & 1 \end{bmatrix}, \quad \mathbf{y} = \begin{bmatrix} y_1 \\ y_2 \\ \vdots \\ y_p \end{bmatrix}, \quad (3.6)$$

where n is the order of the polynomials, and p is the number of points at the mesh.

All the three options can eliminate the oscillations on the eigenfunctions, but we interested in the best choice. This work adopts the Rayleigh Quotient [6] as the error criterion, which for analytic functions can be expressed as

$$\omega_j^2 = \frac{\int_0^l EI (d^2 \varphi_j / dx^2)^2 dx}{\int_0^l \rho a \varphi_j^2 dx}. \quad (3.7)$$

The discrete form is given by $\omega_j^2 = \varphi_j^T \mathbf{K} \varphi_j / \varphi_j^T \mathbf{M} \varphi_j$, where in this case φ_j are the eigenvectors.

In this work we tested the numerical implementation of three approximation schemes proposed. Results show that they can eliminate oscillations but with different effects on the Rayleigh Quotient. Figure 2 shows the smoothed resulting mode shape, free from the oscillations for the mixed Lagrange-Hermite formulation.

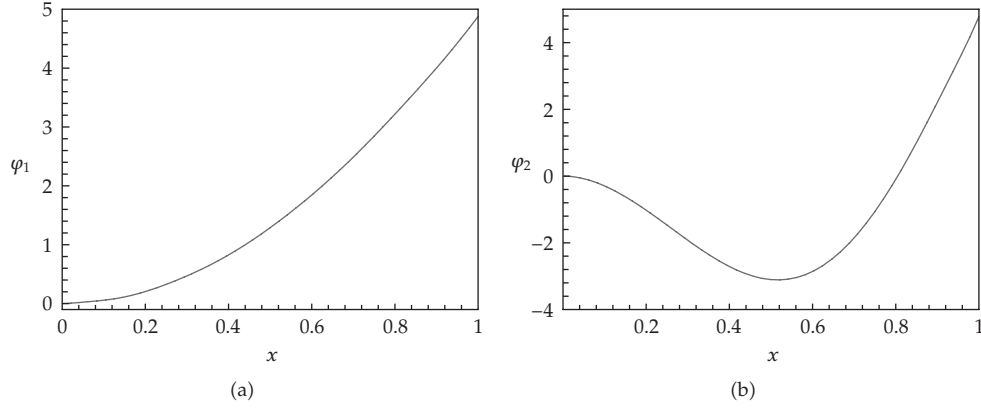


Figure 2: Eigenfunctions which represent the vibration modes of a link fixed on $x = 0$. (a) is the first mode and (b) the second mode. Eigenfunctions generate through the interpolation with mixed Lagrange-Hermite polynomials.

The eigenvalue error of the smoothed eigenvectors in (3.7) and the original eigenvalues from (3.5) are around 1 Hz for the first and the second mode and 2 Hz for the third mode, which means around 5% for the first vibration mode and smaller for the second and third.

For the links geometries tested in this work, the complete Hermite approximation gave smaller eigenfunctions errors, but other geometries might have better results with other approximation schemes.

4. Equations of Motion

The closed form equations of motion are derived using a Lagrangian approach, written as

$$\frac{d}{dt} \left(\frac{\partial L}{\partial \dot{q}_i} \right) - \frac{\partial L}{\partial q_i} = F_i, \quad i = 1, 2, \dots, n+m, \quad (4.1)$$

where $L = T - U$ is the Lagrangian, T is the kinetic energy, U is the potential energy, q_i are the generalized coordinates, associated with joint coordinates and link deflections, and F_i are the generalized forces. In the form of compact matrices [10], it can be written as

$$\mathbf{B}(\mathbf{q})\ddot{\mathbf{q}} + \mathbf{C}(\mathbf{q}, \dot{\mathbf{q}})\dot{\mathbf{q}} + \mathbf{K}_e\mathbf{q} + \mathbf{D}\dot{\mathbf{q}} + \mathbf{g}(\mathbf{q}) = \mathbf{u}, \quad (4.2)$$

where $\mathbf{q} = [\boldsymbol{\theta}, \boldsymbol{\delta}]^T$ is the generalized coordinates vector, $\boldsymbol{\theta}$ is the $n \times 1$ joint coordinates vector, $\boldsymbol{\delta}$ is the $m \times 1$ elastic modes coordinates vector, $\mathbf{B}(\mathbf{q})$ is the positive definite symmetric inertia matrix, $\mathbf{C}(\mathbf{q}, \dot{\mathbf{q}})$ is the Coriolis and centrifugal forces vector, $\mathbf{g}(\mathbf{q})$ is the gravitational torque vector, \mathbf{K}_e is the positive definite stiffness diagonal matrix, \mathbf{D} is the positive semidefinite link diagonal damping matrix, and \mathbf{u} is the joint input torque vector.

The various matrices from the dynamic model can be partitioned as

$$\begin{aligned} \mathbf{B}(\mathbf{q}) &= \begin{bmatrix} \mathbf{B}_{\theta\theta} & \mathbf{B}_{\theta\delta} \\ \mathbf{B}_{\theta\delta}^T & \mathbf{B}_{\delta\delta} \end{bmatrix}, & \mathbf{C}(\mathbf{q}, \dot{\mathbf{q}}) &= \begin{bmatrix} \mathbf{C}_{\theta\theta} & \mathbf{C}_{\theta\delta} \\ \mathbf{C}_{\delta\theta} & \mathbf{C}_{\delta\delta} \end{bmatrix}, & \mathbf{K}_e &= \begin{bmatrix} 0 & 0 \\ 0 & \mathbf{K} \end{bmatrix}, \\ \mathbf{g}(\mathbf{q}) &= \begin{bmatrix} \mathbf{g}_\delta(\boldsymbol{\theta}) \\ \mathbf{g}_\theta(\boldsymbol{\delta}) \end{bmatrix}, & \mathbf{u} &= \begin{bmatrix} \boldsymbol{\tau} \\ 0 \end{bmatrix}, \end{aligned} \quad (4.3)$$

where the indices $\theta\theta$, $\delta\theta$, and $\delta\delta$ are the terms from the matrices corresponding with rigid body, rigid coupling with flexible body, and flexible body, respectively.

5. Tracking Control

This section introduces the flexible robot arm tracking control, presented by [3]. The algorithm uses an adaptive control for joint tracking and a robust control law to reduce the elastic vibrations of the arms. The improved tracking controller using nominal compensation of dynamic nonlinearities of system equation (4.2) is given by

$$\mathbf{u} = \mathbf{B}(\mathbf{q})\ddot{\mathbf{q}}_r + \mathbf{C}(\mathbf{q}, \dot{\mathbf{q}})\dot{\mathbf{q}}_r + \mathbf{K}_e\mathbf{q}_d + \mathbf{D}\dot{\mathbf{q}}_r + \mathbf{g}(\mathbf{q}) - \mathbf{K}_p\mathbf{s}, \quad (5.1)$$

where \mathbf{K}_p is the positive definite diagonal gain matrix, $\dot{\mathbf{q}}_r = \dot{\mathbf{q}}_d - \boldsymbol{\Lambda}\tilde{\mathbf{q}}$ is the reference velocity vector, with tracking error $\tilde{\mathbf{q}} = \mathbf{q} - \mathbf{q}_d$, \mathbf{q} is the robot path, \mathbf{q}_d is the desired path and $\mathbf{s} = \dot{\mathbf{q}} - \dot{\mathbf{q}}_r = \dot{\tilde{\mathbf{q}}} + \boldsymbol{\Lambda}\tilde{\mathbf{q}}$ is the reference error, and $\boldsymbol{\Lambda}$ is a diagonal gain matrix.

Inserting (5.1) in the dynamics equation (4.2), the error equation becomes

$$\mathbf{B}(\mathbf{q})\dot{\mathbf{s}} = -(\mathbf{C}(\mathbf{q}, \dot{\mathbf{q}})\mathbf{s} + \mathbf{K}_e\tilde{\mathbf{q}} + \mathbf{D}\mathbf{s} + \mathbf{K}_p\mathbf{s}). \quad (5.2)$$

In order to prove the stability at the origin of (5.2), consider $\mathbf{x} = [\tilde{\mathbf{q}} \ \dot{\tilde{\mathbf{q}}}]^T$ with the Lyapunov function

$$\mathbf{V}(\mathbf{x}, t) = \mathbf{V}(\mathbf{x}) = \frac{1}{2}\mathbf{s}^T\mathbf{B}(\mathbf{q})\mathbf{s} + \tilde{\mathbf{q}}^T(\boldsymbol{\Lambda}\mathbf{K}_p + \mathbf{K}_e)\tilde{\mathbf{q}}. \quad (5.3)$$

Differentiating (5.3) along (5.2), and using the skew symmetric property of $\mathbf{B}(\mathbf{q}) - 2\mathbf{C}(\mathbf{q}, \dot{\mathbf{q}})$ that implies $\mathbf{s}^T(\mathbf{B}(\mathbf{q}) - 2\mathbf{C}(\mathbf{q}, \dot{\mathbf{q}}))\mathbf{s} = 0$ [14], it results

$$\dot{\mathbf{V}}(\mathbf{x}) = -\dot{\tilde{\mathbf{q}}}^T\mathbf{K}_p\tilde{\mathbf{q}} - \tilde{\mathbf{q}}^T(\boldsymbol{\Lambda}\mathbf{K}_p + \mathbf{K}_e)\tilde{\mathbf{q}}. \quad (5.4)$$

Since \mathbf{K}_p , $\boldsymbol{\Lambda}$, and \mathbf{K}_e are diagonal positive definite matrices, then $\dot{\mathbf{V}}(\mathbf{x}) \leq 0$, which implies that the equilibrium point $\mathbf{x} = 0$ is asymptotically stable [3]. However, it is not

guaranteed that the deflections tend to zero for weakly damped system. In this case, we can add a robust control law [2], that damps the system and eliminate the steady vibrations as

$$\begin{aligned} \mathbf{D}'_{\Delta} \dot{\boldsymbol{\delta}}_d &= (\mathbf{D}_{\Delta} - \text{diag}\{f_{11}, \dots, f_{1r_1}, \dots, f_{nr_1}, \dots, f_{nr_n}\}) \dot{\boldsymbol{\delta}}_d, \\ f_{ij} &= \frac{\dot{\boldsymbol{\delta}}_{dij} \mathbf{s}_{dij}}{\|\dot{\boldsymbol{\delta}}_{dij} \mathbf{s}_{dij}\| + \epsilon_{ij} e^{-\varphi_{ij}}}, \quad i = 1, \dots, n, j = 1, \dots, r_i, \end{aligned} \quad (5.5)$$

where $\dot{\boldsymbol{\delta}}_{dij}$, \mathbf{s}_{dij} are generic elements dependent on desired deflections $\boldsymbol{\delta}_d$ and tracking error \mathbf{s} , r_i is the number of deflection generalized coordinates for link i , and n is the number of links. The robust control law (5.5) shows strong adaptation to various perturbation from modeling errors and disturbance, and guaranteed transient performance [15].

To prove the stability of the deflections $\boldsymbol{\delta}_i$ we assume that $\boldsymbol{\theta}_d$ is constant, and from (4.2) we reach partitioned equation for a desired deflection $\boldsymbol{\delta}_d$

$$\mathbf{B}_{\delta\delta} \ddot{\boldsymbol{\delta}}_d + \mathbf{C}_{\delta} \dot{\boldsymbol{\delta}}_d + \mathbf{D}'_{\Delta} \dot{\boldsymbol{\delta}}_d + \mathbf{K} \boldsymbol{\delta}_d + \mathbf{g}(\boldsymbol{\delta}_d) = 0. \quad (5.6)$$

Considering $\mathbf{y} = \boldsymbol{\delta}_d + \mathbf{K}^{-1} \mathbf{g}_{\delta}$ in (5.6) results

$$\mathbf{B}_{\delta\delta} \ddot{\mathbf{y}} + \mathbf{C}_{\delta} \dot{\mathbf{y}} + \mathbf{D}'_{\Delta} \dot{\mathbf{y}} + \mathbf{K} \mathbf{y} = 0, \quad (5.7)$$

with Lyapunov function

$$\mathbf{V}_y(\mathbf{y}, \dot{\mathbf{y}}) = \frac{1}{2} \mathbf{y}^T \mathbf{K} \mathbf{y} + \frac{1}{2} \dot{\mathbf{y}}^T \mathbf{B}_{\delta\delta} \dot{\mathbf{y}}. \quad (5.8)$$

Taking the time derivative of (5.8) along (5.7) and using again the property that $\mathbf{B}_{\delta\delta} - 2\mathbf{C}_{\delta}$ is skew symmetric and $\mathbf{y}^T (\mathbf{B}_{\delta\delta} - 2\mathbf{C}_{\delta}) \mathbf{y} = 0$ [14], it results

$$\dot{\mathbf{V}}_y(\mathbf{y}, \dot{\mathbf{y}}) = -\dot{\mathbf{y}}^T \mathbf{D}'_{\Delta} \dot{\mathbf{y}}. \quad (5.9)$$

Since \mathbf{D}'_{Δ} is a diagonal positive definite matrix, then $\dot{\mathbf{V}}_y(\mathbf{y}, \dot{\mathbf{y}}) \leq 0$, which implies that the equilibrium point $\mathbf{y} = 0$ is asymptotically stable.

Equation (5.5) is added to (5.1) to obtain the control law of the system equation (4.2) expressed as

$$\mathbf{u} = \mathbf{B}(\mathbf{q}) \ddot{\mathbf{q}}_r + \mathbf{C}(\mathbf{q}, \dot{\mathbf{q}}) \dot{\mathbf{q}} + \mathbf{K}_e \mathbf{q}_d + \mathbf{D} \dot{\mathbf{q}}_r + \mathbf{g}(\mathbf{q}) - \mathbf{K}_p \mathbf{s} + \begin{bmatrix} 0^T & (\mathbf{D}'_{\Delta} \dot{\boldsymbol{\delta}}_d)^T \end{bmatrix}^T. \quad (5.10)$$

The proof of the stability of this control law can be obtained using Lyapunov stability theory in a similar manner to that shown in the stability of the control law (5.1). So the control law (5.10) is stable on the origin, and tracking error $\tilde{\mathbf{q}}$ tends to zero. The damping of the system has been increased, and the deflection modes tend to zero. A detailed proof of the stability of this control law can be seen in [3].

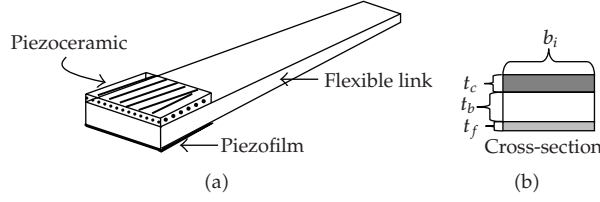


Figure 3: Link nonprismatic and flexible.

6. Piezoelectric Vibration Control

Under certain conditions, achieving the suppression of elastic link vibrations by means of the motor torque alone may be very difficult. Hardware limitations, such as motor saturation and motor noise, may prevent the control of high-frequency vibration modes. To solve these problems we use a hybrid controller consisting of the servomotor and piezoelectric actuators and sensors bonded to the flexible links as shown in Figure 3. This nonprismatic link has a linearly varying cross section.

We propose a vibration feedback control voltage to the piezoceramic actuator based on the voltage of the piezofilm sensor [16], expressed as

$$\mathbf{P}(t) = -\mathbf{c}_a^T \mathbf{K}_c \dot{\mathbf{P}}_f(t) \quad (6.1)$$

with

$$\mathbf{c}_a = \frac{E_b E_c t_c t_f d_{31}}{\rho_b a_b (E_b t_b + 6E_c t_c)} (\varphi'(x_a + a_{pc}) - \varphi'(x_a)), \quad (6.2)$$

where \mathbf{K}_c is the feedback gain, E_c and E_b are the elastic modulus of the piezoceramic and the link, respectively, t_c , t_f , and t_b are the piezoceramic, piezofilm, and link thicknesses, respectively, a_b is the cross section of the link, d_{31} is the piezoelectric constant ρ_b is the mass density, a_{pc} is the size of the actuator, x_a is the localization from the actuator on the link, and $\dot{\mathbf{P}}_f(t)$ is the voltage generated by the piezofilm sensor, obtained by integrating the electric charge developed at a point on the piezofilm, expressed as

$$P_f(t) = c_s \delta = \frac{k_{31}^2 b_f}{C g_{31}} d_{mi} \delta, \quad (6.3)$$

where k_{31}^2 is the electromechanical coupling factor, C is the capacitance of the film sensor, d_{mi} is the distance from the bottom of the piezofilm sensor to the neutral axis, b_f is the width of piezofilm, and g_{31} is the piezoelectric stress constant [17]. This additional controller equation (6.1) is combined to the original one. The resulting control law for the system equation (5.3) is expressed as

$$\mathbf{u} = \mathbf{B}(\mathbf{q})\ddot{\mathbf{q}}_r + \mathbf{C}(\mathbf{q}, \dot{\mathbf{q}})\dot{\mathbf{q}} + \mathbf{K}_e \mathbf{q}_d + \mathbf{D}\dot{\mathbf{q}}_r + \mathbf{g}(\mathbf{q}) - \mathbf{K}_p \mathbf{s} + \begin{bmatrix} 0^T & (\mathbf{D}'_\Delta \dot{\boldsymbol{\delta}}) + c_a P(t) \end{bmatrix}^T. \quad (6.4)$$

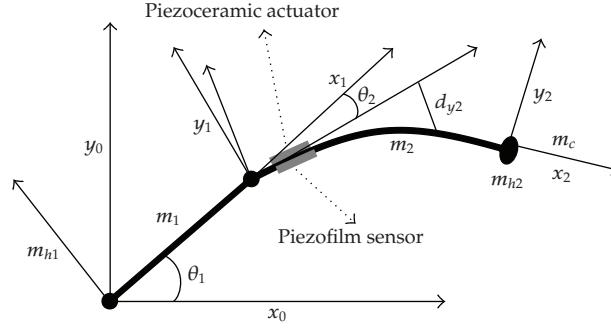


Figure 4: Model of planar one-link flexible manipulator featuring piezoelectric actuators and sensors.

Using Lyapunov stability theory on (6.4) we can prove that the trajectory error and flexible link deflections result asymptotically stable for this control law.

The total potential energy U_e of the flexible manipulator is given by the sum of the elastic energies at each link and can be expressed as

$$U_e = \delta^T \mathbf{K}_e \delta, \quad (6.5)$$

where \mathbf{K} is the generalized stiffness matrix of the links. For a link i

$$\mathbf{K}_i = \int_0^{l_i} (EI)_i \frac{d^2 \varphi_{ij}}{dx_i^2} \frac{d^2 \varphi_{ik}}{dx_i^2} dx_i, \quad (6.6)$$

where j and k are the eigenfunctions index.

The inclusion of the piezoelectric material on the flexible links is accounted by defining the beam properties with Heaviside functions to change the geometry and stiffness where the material is added. The computation of the eigenfunctions for (6.6) is accomplished as shown in Section 3.

7. Results

The physical system considered in this work is composed by a rigid and a flexible link, joints, and motors, based on the robot design suggested by Kim et al. [9] and Bottega et al. [18].

However, this work contains significant improvements with respect to the previously published work [18]. The flexible link geometry was generalized to allow nonprismatic designs. Three vibration modes are used in the simulation, instead of two, while the control is still derived with two modes. The main reason behind this last difference is to test if the control is robust enough to damp the additional mode.

The simplified model robot with the first rigid and the second flexible link is shown in Figure 4. Gravitational effects were ignored [19]. The Lagrangian coordinate vector is $\mathbf{q} = [\theta_1, \theta_2, \delta_1, \delta_2, \delta_3]^T$.

The results were obtained using a block-diagram implemented in MatLab/Simulink software presented in Figure 5, where the fourth-order Runge-Kutta method with $\Delta t = 1$ milliseconds was used to integrate the equations for a five-second simulation.

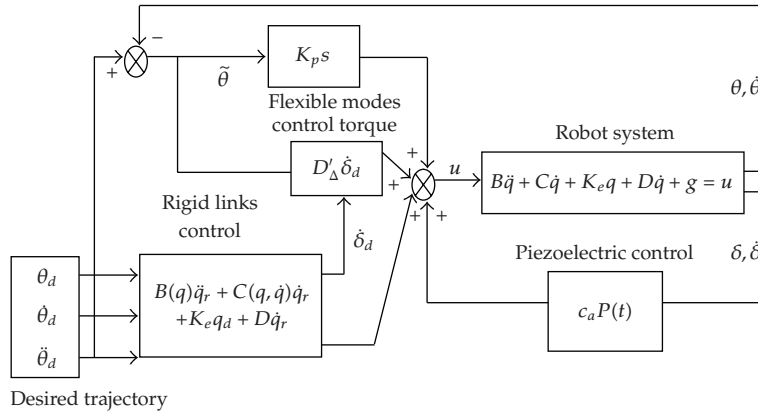


Figure 5: Block-diagram of the proposed control algorithm.

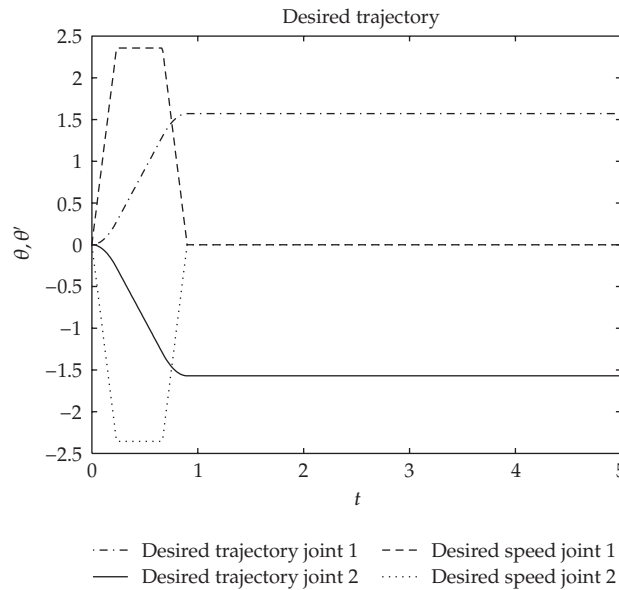


Figure 6: Desired trajectory and speed of the joint angle 1 and 2.

From rigid body dynamics, the torque is proportional to the angular acceleration and the mass inertia. For the second joint, since the inertia is constant, the torque would be a positive constant value for the initial instants, zero for the constant speed period, and negative constant for the deceleration period. For the first joint, the inertia of the second link is changing due to its relative motion; so it is a bit more complicated but is a simple function of the motion [20].

In this system, the torque control for joint angle is obtained through (5.10), which depends on the error path. Because of this, we introduce to control torque a trajectory to the desired angle for the joints 1 and 2. Here we choose a trapezoidal speed trajectory with amplitude $\pi/2$, without initial tracking error was shown in Figure 6.

Table 1: Dimensional and mechanical properties of the aluminium link and piezoelectric materials. Capacitance of the piezofilm (C) 380 pF cm^{-2} . Piezoelectric stress constant of the piezofilm (g_{31}) $216 \times 10^{-3} \text{ (V m}^{-1}) \text{ (N m}^{-2})^{-1}$. Electromechanical coupling factor (k_{31}) 0.44.

	Young's modulus (GPa)	Thickness (mm)	Density (kg m^{-3})	Width (mm)	Length (m)
Aluminum link	65	at one side: 1 at other: 0.6	2890	25	1
Piezoceramic (PZT)	64	0.815	7700	25	0.2
Piezofilm	2.0	0.028	1780	25	0.2

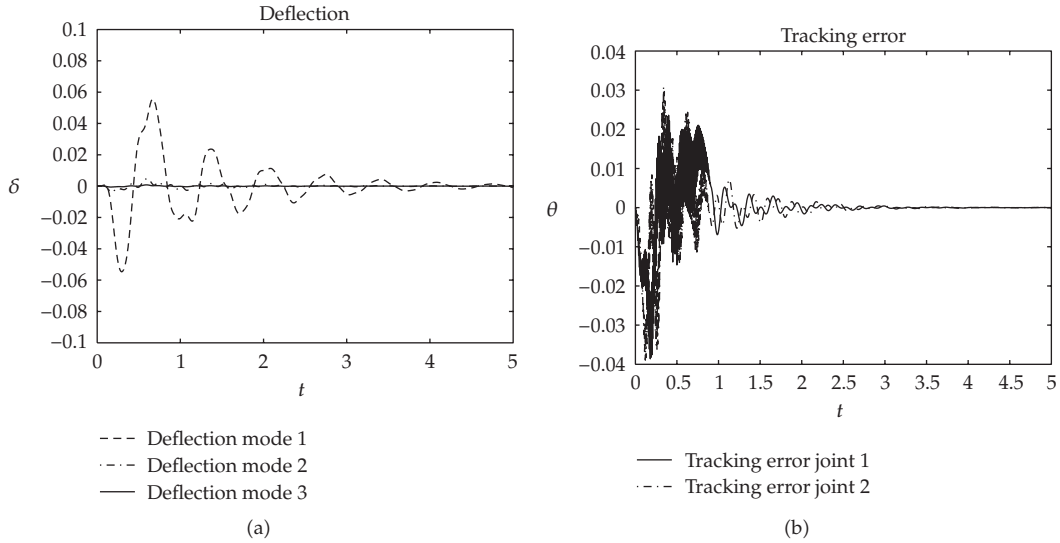


Figure 7: (a) Deflection of first, second, and third modes with damping. (b) Tracking error of the trapezoidal trajectory tracking system.

7.1. Physical Parameters

Table 1 presents the mechanical and geometrical properties of the piezoelectric materials [7, 8] used in this work. The manipulator geometry and masses are the same as in [3].

8. Simulations

Firstly, we simulated a damped system with a control law (5.1). Figure 7(a) shows that the elastic deflections tend to zero, and they are limited due to natural damping of the system. Figure 7(b) shows that the system tracking error also tends to zero.

In the second simulation, we used the control law given by (5.10) in the same system used before. Figure 8(a) shows an increase in the system damping and a faster deflections converge to zero. This is a result of the addition of $D'_\Delta \delta_d$ controller.

For the next simulations of the system with control law (6.4), we added piezoelectric actuators and sensors in the position $x_a = 0.09 \text{ m}$ and sizing $a_{pc} = 0.39 \text{ m}$ of piezoelectric. Figure 8(b) shows a reduction on the frequency and deflection amplitude induced by the tracking control when piezoelectric actuators and sensors are added.

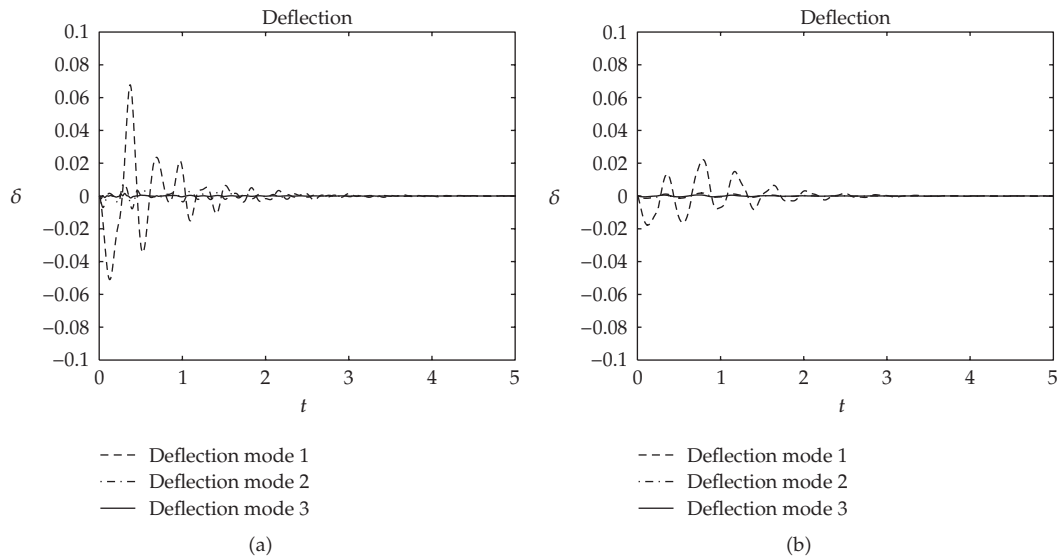


Figure 8: (a) Deflections of first, second, and third modes for damping system with robust control. (b) Deflections of first, second, and third modes for damping system with piezoelectric actuator and sensor.

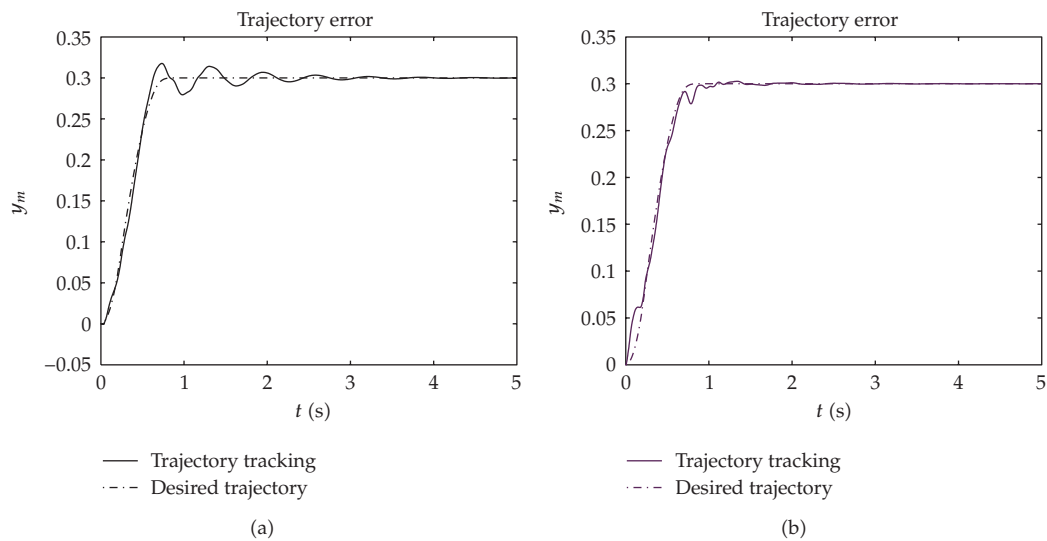


Figure 9: (a) Vertical tip trajectory error with robust control without piezoelectric material. (b) Vertical tip trajectory error with robust control and piezoelectric actuator and sensor.

Figures 9(a) and 9(b) also show a reduction on the trajectory tracking error control when piezoelectric actuators and sensors are added. The robot manipulator starts with both links stretched and ends with the first joint at $\pi/2$ and the second at $-\pi/2$.

Figures 10(a) and 10(b) show a reduction on the frequency and deflection amplitude, in the first mode, induced by the tracking control and when piezoelectric actuators and sensors are added.

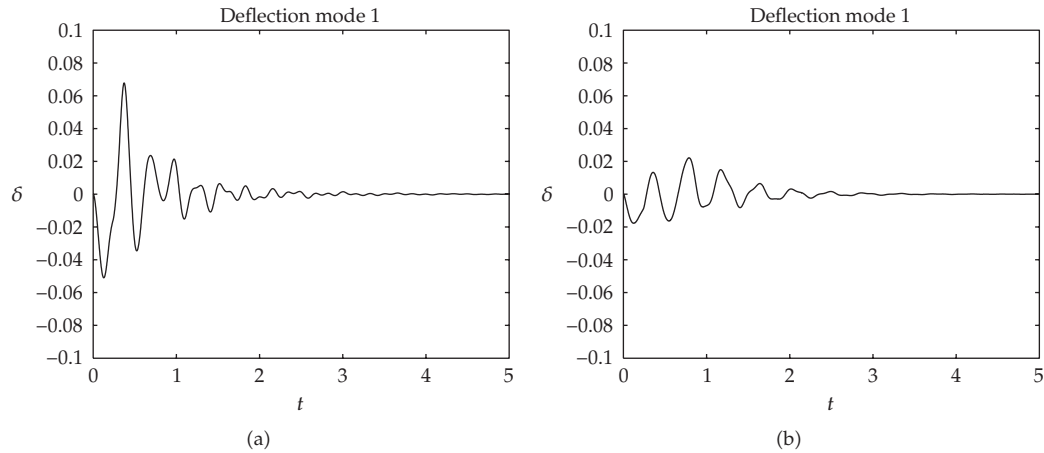


Figure 10: (a) Deflections of first mode for damping system with robust control. (b) Deflections of first mode for damping system with piezoelectric actuator and sensor.

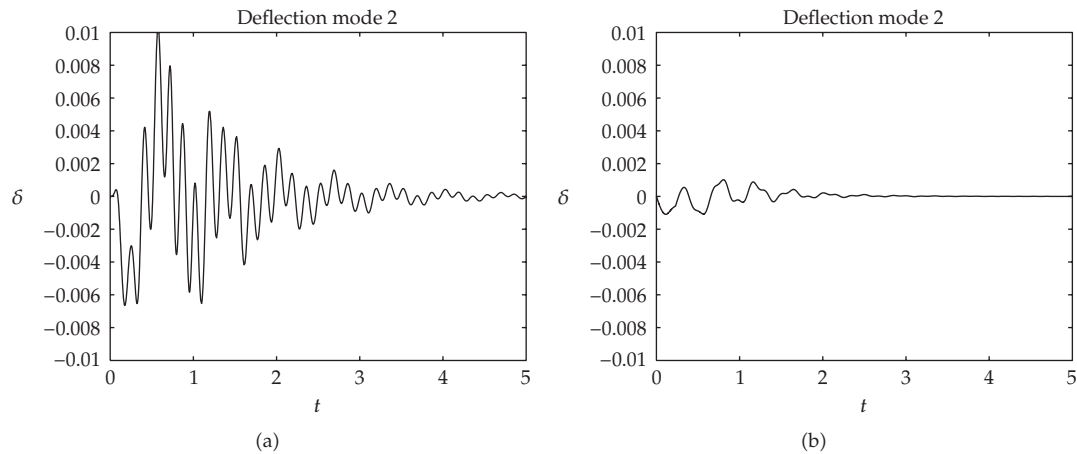


Figure 11: (a) Deflections of second mode for damping system with robust control. (b) Deflections of second mode for damping system with piezoelectric actuator and sensor.

Figures 11(a) and 11(b) show a reduction on the frequency and deflection amplitude, in the second mode, induced by the tracking control and when piezoelectric actuators and sensors are added.

Figures 12(a) and 12(b) show a reduction on the frequency and deflection amplitude, in the third mode, induced by the tracking control and when piezoelectric actuators and sensors are added.

It is clearly seen in Figures 8, 9, 10, 11, and 12 that the frequency and deflection amplitude are reduced by activating the piezoelectric actuators and sensors during the motion. These simulations show competitive results with other published approaches [9].

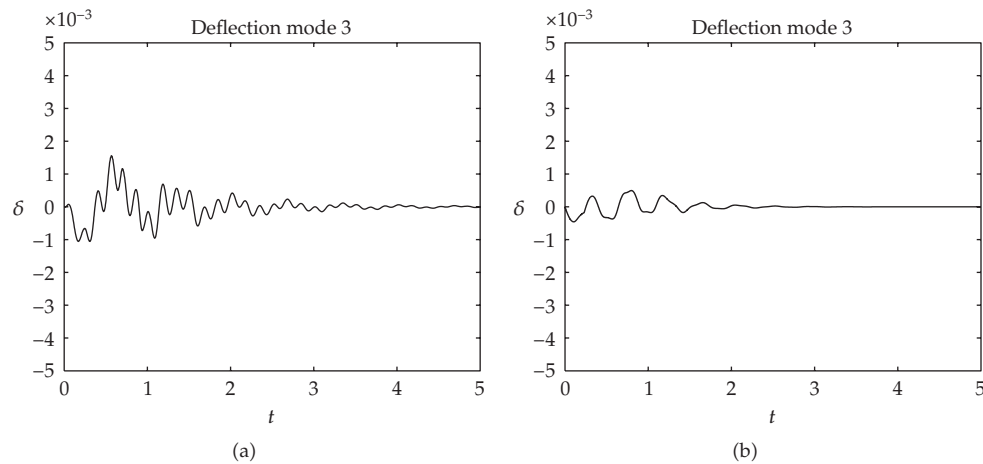


Figure 12: (a) Deflections of third mode for damping system with robust control. (b) Deflections of third mode for damping system with piezoelectric actuator and sensor.

9. Conclusions and Considerations

In this work we presented the derivation of a tracking and vibration control of a robot with flexible links. This technique uses the motor torque for the joint angle control and also for controlling the low-frequency vibrations in the robot links. Piezoelectric actuators and sensors are added to the system to control the high-frequency vibrations that cannot be reduced by the motor alone.

For geometric complex links, the eigenvectors are approximated using polynomial interpolation spanning all finite elements of each flexible link. The Rayleigh quotient was used for the validity of the technique. Hermite polynomials interpolation proved to be the best approximation for this case.

The simulations for the control system confirmed the effectiveness for this control technique. The numerical results indicate that oscillations were suppressed, and the tip trajectory was stabilized.

This methodology can be developed to build light manipulators with flexible links, while preserving the force and precision. It also reduces the energy consumption and suits the needs for aerospace systems or for tasks that demand lightness, precision, and agility.

Acknowledgments

The authors A. Molter and J. S. O. Fonseca would like to acknowledge the financial support by CAPES, Grand PNPD-0055085, and by CNPq, Brasília, Brazil. The authors V. Bottega and R. Pergher acknowledge the support of the CCET-University of Caxias do Sul, Brazil.

References

- [1] V. Bottega, R. Pergher, A. Molter, and J. S. O. Fonseca, "Modelagem, controle e simulação de manipuladores robóticos com braços flexíveis de geometria irregular," in *CMNE CILAMCE Iberian Latin American Congress on Computational Methods in Engineering*, Porto, Portugal, 2007.

- [2] S. Arimoto, *Control Theory of Non-Linear Mechanical Systems*, Oxford Clarendon Press, London, UK, 1996.
- [3] M. A. Arteaga and B. Siciliano, "On tracking control of flexible robot arms," *IEEE Transactions on Automatic Control*, vol. 45, no. 3, pp. 520–527, 2000.
- [4] D. Sun, J. K. Mills, J. Shan, and S. K. Tso, "A PZT actuator control of a single-link flexible manipulator based on linear velocity feedback and actuator placement," *Mechatronics*, vol. 14, no. 4, pp. 381–401, 2004.
- [5] J. K. Bathe and E. L. Wilson, *Numerical Methods in Finite Element Analysis*, Prentice-Hall, Englewood Cliffs, NJ, USA, 1976.
- [6] D. L. Clive and I. H. Shames, *Solid Mechanics: A Variational Approach*, McGraw-Hill, New York, NY, USA, 1973.
- [7] S.-B. Choi and H.-C. Shin, "A hybrid actuator scheme for robust position control of a flexible single-link manipulator," *Journal of Robotic Systems*, vol. 13, no. 6, pp. 359–370, 1996.
- [8] S. B. Choi, S. S. Cho, H. C. Shin, and H. K. Kim, "Quantitative feedback theory control of a single-link flexible manipulator featuring piezoelectric actuator and sensor," *Smart Materials and Structures*, vol. 8, no. 3, pp. 338–349, 1999.
- [9] H.-K. Kim, S.-B. Choi, and B. S. Thompson, "Compliant control of a two-link flexible manipulator featuring piezoelectric actuators," *Mechanism and Machine Theory*, vol. 36, no. 3, pp. 411–424, 2001.
- [10] W. J. Book, "Recursive lagrangian dynamics of flexible manipulator arms," *International Journal of Robotics Research*, vol. 3, no. 3, pp. 87–101, 1984.
- [11] L. Meirovitch, *Analytical Methods in Vibration*, Macmillan, New York, NY, USA, 1967.
- [12] A. de Luca, P. Lucibello, and F. Nicolo, "Automatic symbolic modeling and nonlinear control of robots with flexible links," in *Proceedings of the IEEE Work on Robot Control*, pp. 62–70, Oxford, UK, 1988.
- [13] D. G. Luenberger, "Algorithmic analysis in constrained optimization," in *Nonlinear Programming*, SIAM-AMS Proceedings, vol. 9, pp. 39–51, American Mathematical Society, Providence, RI, USA, 1976.
- [14] M. A. Arteaga, "On the properties of a dynamic model of flexible robot manipulators," *ASME Journal of Dynamics Systems, Measurement, and Control*, vol. 120, no. 1, pp. 8–14, 1998.
- [15] B. Yao and M. Tomizuka, "Smooth robust adaptive sliding mode control of manipulators with guaranteed transient performance," *ASME Journal of Dynamics Systems, Measurement, and Control*, vol. 118, no. 4, pp. 764–775, 1996.
- [16] E. F. Crawley and J. de Luis, "Use of piezoelectric actuators as elements of intelligent structures," *AIAA Journal*, vol. 25, no. 10, pp. 1373–1385, 1987.
- [17] H. T. Banks, R. C. Smith, and Y. Wang, *Smart Material Structures: Modeling, Estimation and Control*, John Wiley & Sons, Paris, France, 1996.
- [18] V. Bottega, R. Pergher, and J. S. O. Fonseca, "Simultaneous control and piezoelectric insert optimization for manipulators with flexible link," *Journal of the Brazilian Society of Mechanical Sciences and Engineering*, vol. 31, no. 2.
- [19] A. de Luca, L. Lanari, P. Lucibello, S. Panzieri, and G. Ulivi, "Control experiments on a two-link robot with a flexible forearm," in *Proceedings of the 29th IEEE Conference on Decision and Control (CDC '90)*, vol. 2, pp. 520–527, Honolulu, Hawaii, USA, 1990.
- [20] L. Sciacivco and B. Siciliano, *Modelling and Control of Robot Manipulators*, Advanced Textbooks in Control and Signal Processing Series, Springer, London, UK, 2nd edition, 2000.